where the term containing Δ_1 accounts for the $i = j$ contribution in the sum

$$\Delta_1 = \left\langle \frac{\partial u(\vec{r}_1)}{\partial f} \frac{\partial u(\vec{r}_2)}{\partial f} \right\rangle - \left\langle \left(\frac{\partial u}{\partial f} \right)^2 \right\rangle \quad \text{(A8)}$$

The averages in eqs A7 and A8 are defined by

$$\left\langle \left(\frac{\partial u}{\partial f} \right)^2 \right\rangle = \frac{1}{Z_0} \int d\vec{r}_1 \ldots d\vec{r}_N \left[\frac{\partial u(\vec{r}_1)}{\partial f} \right]^2 \exp(-\beta U_0) \quad \text{(A9)}$$

and

$$\left\langle \frac{\partial u(\vec{r}_1)}{\partial f} \frac{\partial u(\vec{r}_2)}{\partial f} \right\rangle = \frac{1}{Z_0} \int d\vec{r}_1 \ldots d\vec{r}_N \frac{\partial u(\vec{r}_1)}{\partial f} \frac{\partial u(\vec{r}_2)}{\partial f} \exp(-\beta U_0) \quad \text{(A10)}$$

Substitution of eqs A4, A6, and A7 into eq A1 and application of the identity eq A5 lead to

$$A - A_0 - A_{mix} = N \left\{ \left\langle \frac{\partial u}{\partial f} \right\rangle [x_A(f_A - f_0) + x_B(f_B - f_0)] + \Delta[x_A(f_A - f_0)^2 + x_B(f_B - f_0)^2] + \frac{1}{2}\beta\Delta_1 x_A x_B (f_A - f_B)^2 \right\} \quad \text{(A11)}$$

In the description of the experiment we are interested in differences between the chemical potential of the mixture and a standard chemical potential, which we choose to be the chemical potential for $x_A = 0$. Then the free energy difference of interest is

$$A - A_{mix} - A_{BB} = N x_A \left\{ \left\langle \frac{\partial u}{\partial f} \right\rangle (f_A - f_B) + \Delta[(f_A - f_0)^2 - (f_B - f_0)^2] + \frac{1}{2}\beta\Delta_1(1 - x_A)(f_A - f_B)^2 \right\} \quad \text{(A12)}$$

where

$$\Delta = \frac{1}{2}\left\langle \frac{\partial^2 u}{\partial f^2} \right\rangle - \frac{1}{2}\beta(N-1)\Delta_1 - \frac{1}{2}\beta\left[\left\langle \left(\frac{\partial u}{\partial f} \right)^2 \right\rangle - \left\langle \frac{\partial u}{\partial f} \right\rangle^2 \right] \quad \text{(A13)}$$

Thus, the second-order contribution is partly symmetric and partly antisymmetric under the operation of interchanging A and B. This could provide an explanation of the lack of symmetry in the experiment, if it were not for the universality of the compensation temperature within a compensation class. As has been explained in ref 1, compensation only occurs if one term dominates or if the temperature dependence of all dominating terms is the same. We do not see a physical reason for the temperature dependence of Δ_1 to be the same as the temperature dependence of $\langle \partial u/\partial f \rangle$ or of Δ. Therefore, the asymmetry of the experimental result cannot be explained as a second-order effect of interactions with the resin.

Photophysics of Poly(2,3,4,5,6-pentafluorostyrene) Film

Donald B. O'Connor, Gary W. Scott,*,†

Department of Chemistry, University of California, Riverside, Riverside, California 92521

Daniel R. Coulter, Vincent M. Miskowski, and Andre Yavrouian

Space Materials Science and Technology Section, Jet Propulsion Laboratory, California Institute of Technology, Pasadena, California 91109 *(Received: December 27, 1989)*

The temperature-dependent steady-state emission, emission polarization anisotropy, and fluorescence kinetics of poly(2,3,4,5,6-pentafluorostyrene) film are reported. Two interconverting excited-state conformations of the chromophore have been identified. The fluorescence of the higher energy conformation results from excitation on the red edge of the polymer absorption band at temperatures below 180 K. The energy barrier for conversion of the higher energy conformer to the lower energy conformer is estimated to be $E/hc = 27 \pm 7$ cm^{-1}. Electronic energy migration is not evident in this polymer.

1. Introduction

There has been significant research activity in recent years aimed at understanding the photophysical and photochemical role of electronic energy transfer in long-chain, amorphous polymers containing aromatic pendant chromophores.[1-6] Examples include polystyrene, poly(vinylnaphthalene), and poly(vinylcarbazole). One particular area of concern involves understanding the mechanisms of both photostabilization and photodegradation[7] in such polymeric systems. Photostable polymeric materials are used widely in the solar energy industry especially as coatings for solar collectors, optical elements, and protective containers.[8] We have previously reported on the role of electronic energy transfer in the photophysics of polystyrene copolymerized with a photostabilizing chromophore.[9,10]

The photophysics of these long-chain polymers containing aromatic chromophores are similar in many ways. The absorption spectra of these polymers closely resemble the absorption spectra of their respective chromophores. For example, polystyrene absorption is much like a monoalkyl-substituted benzene absorption. This observation is indicative of weak interaction in the ground

† NASA-ASEE Summer Faculty Fellow, Jet Propulsion Laboratory, 1988 and 1989.

(1) O'Connor, D. B.; Scott, G. W. Laser Studies of Energy Transfer in Polymers Containing Aromatic Chromophores. In *Applications of Lasers in Polymer Science and Technology*; Fouassier, J. P., Rabek, J. Eds.; CRC Uniscience: Boca Raton, FL, in press.

(2) Guillet, J. *Polymer Photophysics and Photochemistry: An Introduction to the Study of Photoprocesses in Macromolecules*; Cambridge University Press: London, 1985.

(3) Phillips, D. Ed. *Polymer Photophysics: Luminescence, Energy Migration and Molecular Motion in Synthetic Polymers*; Chapman and Hall: London, 1985.

(4) Kloepffer, W. *Aromatic Polymers in Dilute Solution. Electronic Energy Transfer and Trapping*; ACS Symp. Ser. 358 (Photophys. Polym.); American Chemical Society: Washington, DC, 1987; pp 264–285.

(5) MacCallum, J. R. *Significance of Energy Migration in the Photophysics of Polystyrene*; ACS Symp. Ser. 358 (Photophys. Polym.); American Chemical Society: Washington, DC, 1987; pp 301–307.

(6) Fredrickson, G. H.; Andersen, H. C.; Frank, C. W. Electronic Excited-State Transport and Trapping on Polymers Chains. *Macromolecules* **1984**, *17*, 54–59.

(7) Ranby, B.; Rabek, J. F. *Photodegradation, Photooxidation, and Photostabilization of Polymers: Principles and Applications*; Wiley: New York, 1975.

0022-3654/90/2094-6495$02.50/0

electronic state between the chromophores of the polymer. The emission spectra of these polymers often exhibits two distinct emission bands. The higher energy band is usually quite similar to the emission from the pertinent monomeric chromophore in dilute solution and is generally attributed to an isolated, noninteracting pendant chromophore, termed the "monomer". For example, polystyrene, both in neat film and in solution exhibits an emission band centered near 290 nm which is very similar to an ethylbenzene emission in dilute solution. The second, lower energy emission band is a Stokes-shifted, structureless band very similar to that described as excimer emission for the respective chromophore in concentrated solution. For example, the excimer emission of benzene is very much like the lower energy emission band of polystyrene.[11] Excimer emission in these polymers arises from the excited-state attractive interaction of two adjacent chromophores during the excited-state lifetime. Such an excimer in a polymer may be formed between two chromophores on the same backbone (an intramolecular excimer), or between two chromophores on spearate macromolecules (an intermolecular excimer). In either case, the chromophores must be quite close spatially since excimer distances between interacting chromophores are typically 3.5 Å.[12,13]

Electronic energy migration refers to the series of energy-transfer processes by which the electronic excitation initially localized on one particular monomer of the polymer is transferred in steps to other chromophores. During each of the energy-transfer steps the excitation is localized on a single chromophore for some short, but finite period of time. This situation is distinctly different from that in which energy is delocalized over many chromophores at the same time such as occurs in organic molecular crystals and is modeled by exciton theory.[14] Since an excimer-forming site produces a relatively low energy species, further energy transfer from it is unlikely, and it is therefore referred to as a trap. Dissociation of the excimer to form an excited-state monomer and a ground-state monomer is, in general, thermodynamically unfavorable. The monomer emission of polystyrene is believed to be principally due to chromophores whose homogeneous absorption bands lie at the red edge of the inhomogeneously broadened absorption band of the amorphous polymer. These states are also expected to be relatively efficient in "trapping" the electronic excitation.

The photophysics of fluorinated benzenes has been investigated rather systematically from monofluorinated benzene to hexafluorobenzene.[15-22] The lowest energy, gas-phase electronic absorption band of all of the fluorinated benzenes has its origin in the wavelength region of 265–275 nm, just as in the case of benzene. The absorption spectra of these molecules exhibit well-resolved vibronic structure in all cases of the mono- and difluorinated benzenes. This vibronic resolution declines rather systematically with further increases in the number of fluorines. The relative positions of the fluorines also affect the observed vibronic structure of the spectra for three or more fluorine substitutions. Virbonic structure is not at all apparent in the gas-phase absorption spectra of either pentafluorobenzene or hexafluorobenzene. The emission spectra of the mono- and difluorinated benzenes are similar to that of benzene in that they consist of a fluorescence band with a Franck–Condon maximum near 290 nm and of well-resolved vibronic transitions. As the number of fluorines increases, the resolution of the emission bands into vibronic bands decreases. In the case of hexafluorobenzene and pentafluorobenzene, the steady-state, gas-phase, room temperature fluorescence spectra of both consist of a broad, structureless, greatly Stokes shifted band with a maximum near 375 nm. Reports of the excited-state decay kinetics of pentafluorobenzene give distinctly different values of the excited-state lifetime.[19,20,22,23] However, it is clear that the emissive excited states of both pentafluorobenzene and hexafluorobenzene are significantly distorted from the ground-state geometry and that they are formed rapidly, in less than 10 ps.

We report here the results of a investigation into the photophysics of the ring-perfluorinated analogue of polystyrene, poly(2,3,4,5,6-pentafluorostyrene), in a neat film. These results increase our understanding of electronic energy migration in polymers containing aromatic pendant chromophores. Additionally, these experiments also offer new insight into the photophysics of pentafluorobenzene and hexafluorobenzene.

2. Experimental Section

2.1. Materials. The 2,3,4,5,6-pentafluorostyrene was obtained from PCR Speciality Chemicals. This monomer was purified by washing with 10% sodium hydroxide and water, dried, and distilled. The polymer was prepared by 2,2′-azobisisobutyronitrile (AIBN)-initiated bulk polymerization. Poly(2,3,4,5,6-pentafluorostyrene) (PPFS) was precipitated three times from ethyl acetate/methanol and further purified by Soxhlet extraction with methanol. The molecular weight was determined by HPLC using tetrahydrofuran (THF) as a solvent and polystyrene standards. It was found to be M_w = 431 000 and M_n = 278 000. Most films were cast from ethyl acetate and were typically 50–100 μm thick. Thinner films (~0.2 μm thick) were spin cast from butyl acetate on sapphire substrates.

Pentafluorotoluene (Aldrich, 99%), ethyl acetate (Aldrich, spectrophotometric grade), and pentane (Mallinckrodt, Spectra AR) were purified by passing through a column of activated alumina (MCB, 80–200 mesh). The synthesis and casting of the polystyrene (PS) film has been described previously.[9]

2.2. Methods. 2.2.1. Absorption, Emission, and Emission Excitation Spectra. The UV absorption spectra were obtained with either a photodiode array spectrometer (Hewlett Packard model 8451A) or a dual beam scanning spectrometer (Varian DMS100). Solutions were contained in a quartz cell of 1 cm path length. The same cell containing only the solvent was used as a reference.

(8) Gebelin, C. G.; Williams, D. K.; Deanin, R. D. Eds. *Polymers in Solar Energy Utilization*, ACS Symp. Ser. 220; American Chemical Society: Washington, DC, 1983.
(9) Coulter, D. R.; Gupta, A.; Yavrouian, A.; Scott, G. W.; O'Connor, D. B.; Vogl, O.; Li, S.-C. Electronic Energy Transfer and Quenching of Copolymers of Styrene and 2-(2′-Hydroxy-5′-vinylphenyl)-2*H*-benzotriazole: Photochemical Processes in Polymeric Systems. 10. *Macromolecules* **1986**, *19*, 1227–1234.
(10) O'Connor, D. B.; Scott, G. W.; Coulter, D. R.; Gupta, A.; Webb, S. P.; Yeh, S. W.; Clark, J. H. Direct observation of the excited state proton transfer and decay kinetics of internally hydrogen bonded photostabilizers in copolymer films. *Chem. Phys. Lett.* **1985**, *121*, 417–422.
(11) Hirayama, F.; Lipsky, S. Excimer fluorescence of benzene and its alkyl derivatives—concentration and temperature dependence. *J. Chem. Phys.* **1969**, *51*, 1939–1951.
(12) Stevens, B. Effects of molecular orientation on fluorescence emission and energy transfer in crystalline aromatic hydrocarbons. *Spectrochim. Acta* **1962**, *18*, 439.
(13) Vala, M. T.; Haibig, J.; Rice, J. A. Experimental study of luminescence and excitation trapping in vinyl polymers, paracyclophanes and related compounds. *J. Chem. Phys.* **1965**, *43*, 886.
(14) Davydov, A. S. *Theory of Molecular Excitons*, Plenum Press: New York, 1971.
(15) Pottier, R.; Semeluk, G. P. Spectrophotometric Studies of the Fluorinated Benzenes in the Near and Far UV. *Can. J. Spectrosc.* **1976**, *21*, 83–95.
(16) Suijker, J. L. G.; Van Tol, M. W.; Huizer, A. H.; Varma, C. A. G. O. An investigation of transient absorptions and a streak camera study of the fluorescence generated by UV excitation of hexafluorobenzene. *J. Photochem.* **1985**, *31*, 165–178.
(17) Suijker, J. L. G.; Varma, C. A. G. O.; Huizer, A. H. Relaxation behavior of electronically excited states of hexafluorobenzene. *J. Mol. Struct.* **1984**, *114*, 269–275.
(18) Phillips, D. Substituent effects in the photochemistry of benzene vapour. *J. Photochem.* **1972/73**, *1*, 97–146.
(19) Brown, R. G.; Phillips, D.; Das Gupta, G. Mechanisms of electronic energy transfer in the gas phase. *J. Phys. Chem.* **1974**, *78*(*23*), 2407–2414.
(20) Brown, R. B.; Phillips, D. Quenching of the first excited singlet state of substituted benzenes by molecular oxygen. *J. Chem. Soc., Faraday Trans. 2* **1974**, *70*, 630–636.
(21) Breuer, G. M.; Lee, E. K. C. Fluorescence decay times and non-radiative decay rates of the first excited singlet states of methylated and fluorinated benzenes. *Chem. Phys. Lett.* **1972**, *14*, 404–406.
(22) Loper, G. L.; Lee, E. K. C. Fluorescence decay and radiative lifetimes of fluorinated aromatic molecules. *Chem. Phys. Lett.* **1972**, *13*, 140–143.
(23) O'Connor, D. V.; Sumitani, M.; Morris, J. M.; Yoshihara, K. Non-exponential picosecond fluorescence decay in isolated pentafluorobenzene and hexafluorobenzene. *Chem. Phys. Lett.* **1982**, *93*, 350–354.

The steady-state emission spectra were obtained with a spectrofluorimeter (Spex Fluorolog 2, Model F212) equipped with double grating emission and excitation monochromators, a high-pressure xenon lamp for excitation, a quantum counter (R6G as scintillator) to monitor the excitation beam intensity, and a photomultiplier tube (Hamamatsu R928-P) in a water-cooled housing operated in photon-counting mode to monitor the emission intensity. The linear reciprocal dispersion of the instrument is 1.8 nm/mm. The emission was collected at either a 90° or a 22° angle relative to the excitation axis. Nonfluorescing filters (Schott KV) were used to eliminate interference of higher orders of either the scattered excitation wavelength or shorter wavelength emission as needed. Each spectrum was corrected for fluctuations in the excitation intensity as well as the wavelength dependence of the detector response.

The temperature variation (10–300 K) of the samples was accomplished with a closed-cycle helium refrigerator (Air Products, Displex 202E) complete with a temperature indicator and controller (Air Products, Model 3700). The polymer films were sandwiched between two sapphire windows mounted in a copper holder that was in thermal contact with the cold stage of the refrigerator. A piece of indium wire was pressed between the cold stage and the copper holder to ensure good thermal contact. A chromel vs gold 0.07% iron thermocouple was attached to the cold stage to record the temperature of the stage while obtaining emission spectra. In order to determine the temperature difference between the cold stage and the sample, a similar thermocouple was embedded in a sample and the voltage difference between the two thermocouples was monitored continuously. The voltage was found to vary by less than 100 μV over the range of 30–300 K and less than 50 μV below 30 K. We estimate all temperatures reported to be correct within ±1.5 K. The sample compartment of the refrigerator was inserted into the sample compartment of the spectrofluorimeter described above to record temperature-dependent steady-state emission spectra. The films were held under vacuum for a minimum of 2 h and usually overnight in the closed-cycle refrigerator at room temperature prior to cooling for experiments.

The emission spectra at temperatures from 2 to 4.2 K were obtained by immersion of the samples in a liquid helium Dewar. Temperatures were varied by reducing the helium gas pressure over the boiling liquid.

2.2.2. Steady-State Emission Spectra Anisotropy. The polarization anisotropy of the steady-state emission spectra was obtained with the spectrofluorimeter described above by adding a calcite Glan-Taylor prism polarizer inserted in the excitation beam and a UV-transmitting sheet polarizer (Optics for Reserach PUM-51) inserted as an analyzer in the emission optical path. The steady-state emission polarization anisotropy is defined by the following expression:

$$r = (I_{VV} - GI_{VH})/(I_{VV} + 2GI_{VH}) \quad (1)$$

in which $G = I_{HV}/I_{HH}$. In this expression, r is the polarization anisotropy and I is emission intensity. The subscripts H and V refer to horizontal and vertical polarization, respectively. The first subscript refers to the polarization of the excitation beam while the second subscript refers to the polarization of the monitored emission. A polarization scrambler was placed immediately after the emission analyzer to minimize deviation of the correction factor G from unity. Experimentally, G varied between 1.0 and 1.05. Scattering from a dilute solution of glycogen (Aldrich, oyster Type II) in water or nondairy creamer (Cremora) in water was used to precisely align the polarizers in the horizontal and vertical positions. The emission was collected at an angle of 90° with respect to the excitation axis. The polymer film, held at 45° with respect to the excitation beam, was sandwiched between a sapphire disk on the backside relative to the excitation beam and a thin copper disk on the front side with a central portion removed to allow direct front surfact excitation. A sapphire disk was not used on the front surface as in the case of collecting emission spectra (see section 2.2.1) because of the crystalline nature of sapphire, and, hence, its depolarizing effect. Otherwise, temperature variation and the recording of spectra were accomplished as described in section 2.2.1.

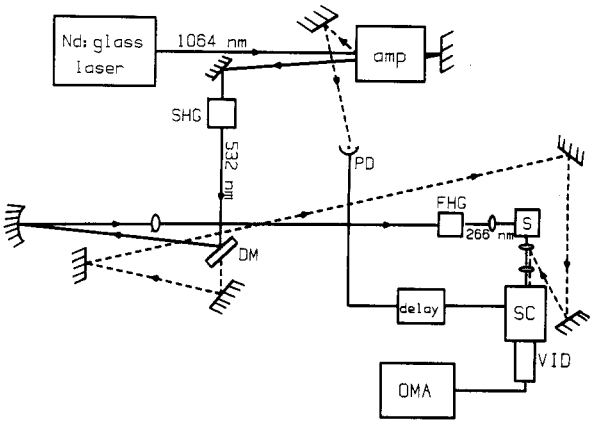

Figure 1. Fluorescence kinetics apparatus. A mode-locked $Nd:^{3+}$ glass laser, double-pass amplifier rod, second harmonic generation crystal (SHG), dichroic mirror (DM), fourth harmonic generation crystal (FHG), sample (S), streak camera (SC), vidicon tube (VID), optical multichannel analyzer (OMA), photodiode (PD), electronic delay box (delay). The marker or prepulse is indicated by the dashed line.

2.2.3. Fluorescence Kinetics. 2.2.3.1. Apparatus. The experimental apparatus used to obtain the fluorescence decay profiles of the polymer film is shown in Figure 1. The sample was excited with a vertically polarized, fourth-harmonic pulse (Δt = 10 ps; λ = 266 nm) from a mode-locked Nd^{3+}:glass laser system. The polymer film was contained in the closed-cycle helium refrigerator as described above (section 2.2.1). The surface normal of the film was held at an angle of approximately 45° with respect to the incident excitation axis. The fluorescence was viewed at 90° with respect to the incident excitation axis thorugh a UV-transmitting sheet polarizer set to pass linearly polarized light at the "magic angle" of 54.7° with respect to the incident pulse polarization. The fluorescence was observed through a nonfluorescing filter (high-energy wavelength cutoff = 418 nm) by an ultrafast streak camera (Hamamatsu C979). The streak was initiated by directing a portion of the fundamental pulse (λ = 1064 nm), reflected off the laser amplifier rod, to a fast pin photodiode (Hamamatsu C1083). The subsequent electronic pulse from the photodiode was sent to the streak camera after an appropriate timing delay (Hamamatsu delay box C1097) and initiated the streak. A portion of the second harmonic pulse transmitted by the harmonic beamsplitter (BS2 in Figure 1) was directed to the streak camera so as to arrive shortly before the fluorescence of the sample. This prepulse acts as a timing marker to assist in signal averaging as discussed below. Streak traces were imaged onto a two-dimensional (512 × 512 channels) vidicon detector (EG&G PARC Model 124E). The digitized output from the vidicon tube was displayed on an OMA (EG&G PARC Model 1216 controller and Model 1215 processor).

2.2.3.2. Streak Camera Calibration. The digitized output displayed on the OMA is a plot of counts per channel. There are 500 channels. The number of counts in each channel can be generally expressed as

$$C = IRT + B \quad (2)$$

in which C is counts, I is the emission intensity of the sample in photons per second, R is the response function of the channel in units of counts per photon, T is the channel time, and B is the background dark counts. The emission intensity I is directly related to the sample kinetics. Therefore, we need to determine B, R, and T in order to obtain I from C. These determinations are discussed below.

The background dark signal B was found generally to increase slowly during the course of a day's experiments. Therefore, immediately upon collection of a decay profile, a background file was taken by blocking the excitation beam immediately after the SHG crystal. This background file was then subtracted from the

decay file. This yields $C - B = IRT$ in the above expression.

The nonlinearity of the sweep speed causes distortion in the time axis and, thus, variation in the channel time T. Determining the channel time T for each channel at a given sweep speed was accomplished with the aid of an etalon constructed from two highly reflective mirrors ($R > 95\%$ at 532 nm) and aluminum spacers of precisely known length. The streak image resulting from passing a second harmonic pulse from the laser system through the etalon consisted of a series of peaks separated in time by $t = 2d/c$, where d is the etalon spacing and c is the speed of light in air. The channel positioned midway between two successive peaks separated by N channels of the streak was assigned a channel time given by t/N. This process was repeated until approximately 250 channel times distributed more or less uniformly across the 500 channels of the streak were assigned. A linear least-squares fit of a multiple order (up to sixth order) polynomial to this data set of channel times was then performed.[24] The resulting best fit was used to obtain the channel time T for each of the 500 channels at a given sweep speed.

It should be noted that the nonlinearity of the sweep speed causes distortion not only in the time axis but also the intensity values. In all but the first 50 channels of the sweep speed used in these experiments, the nonlinearity of the sweep was not sufficient to affect the assignment of the peak positions of the etalon traces. Only data imaged on the last 450 channels of the sweep display were utilized in these experiments.

The intensity response of the channels is nonuniform due to a number of factors including the variation in quantum efficiency across the photocathodes of both the vidicon and streak camera. Additionally, the particular optical arrangement was found to effect the decay profile of a sample. In order to obtain the factor R of eq 2, a fluorescence standard whose decay time was known was utilized. Briefly, the functional form of the standard's decay can be used to generate I in eq 2 for each channel. It is then a straightforward process to extract R from the experimentally obtained profile of the standard. This decay profile of the standard was collected with an identical optical configuration of the apparatus as used to obtain the sample decay profile. In our laboratory a 10^{-6} M solution of rhodamine 6G in methanol whose fluorescence lifetime[25] is 3.9 ± 0.1 ns was used as a fluorescence standard.

2.2.3.3. Data Manipulation. Immediately upon collecting a fluorescence decay profile, a background file was obtained by blocking the laser pulse immediately prior to the SHG crystal. The background file was subtracted from the decay file on the OMA. Several more, usually 5–10, additional decay profiles of the same sample were collected and the background subtracted. Each of these files was then normalized to the maximum intensity value of all the files. These resulting files were subsequently transferred to a microcomputer (Hewlett Packard 87) where they were converted from counts-per-channel files to counts-per-time interval files. This was accomplished by using the calibrated time-per-channel values described in the section 2.2.3.2. The files were then corrected for the nonuniformity of the response utilizing a standard fluorescence decay file obtained with the same optical configuration (see section 2.2.3.2).

Due to the trigger jitter of the streak camera, the onset of the fluorescence profile varied from file to file. In order to sum two or more files for signal averaging, it is necessary to align the marker pulses since the time difference between the marker pulse and the onset of the fluorescence profile is constant in time, being fixed by the optical arrangement. However, this is not straightforward due to the variable channel time across the 500 vidicon channels. In order to facilitate this summing of files, each of the files consisting of intensity per variable time interval was converted to a file of intensity per constant time interval. The constant time interval is simply the sum of all 500 channel times

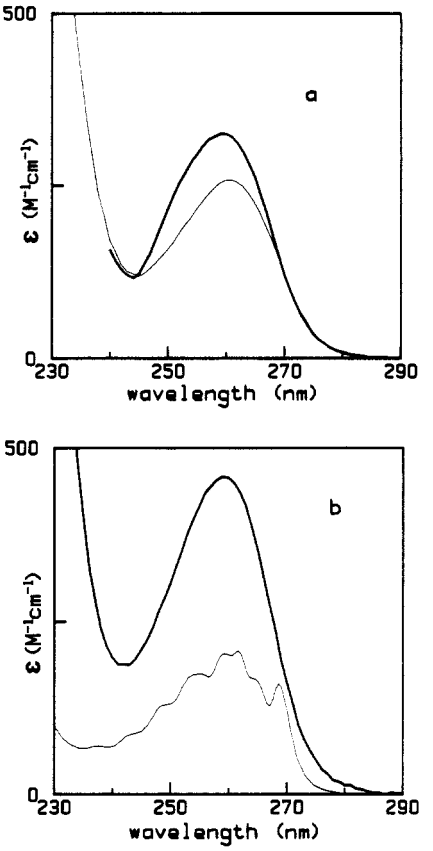

Figure 2. (a) Absorption spectra of PPFS film (light—) and dilute solution of PPFS in ethyl acetate (bold —). The ordinate scale is relative intensity for the PPFS film spectrum. (b) Absorption spectra of 10^{-5} M PFT in pentane (bold —) and polystyrene in cyclohexane (phenyl unit concentration of 10^{-3} M) (light —).

T divided by the number of channels, 500. The intensity values in this new file are obtained by interpolating from the values of the existing file after taking into account the effect of the variable channel times on the intensity values. Two of these resulting files were then summed by simply shifting one file such that its marker pulse maximally overlapped the marker pulse of the other. This summing could be repeated for any number of files.

2.2.3.4. Data Analysis. It was assumed that the fluorescence of PPFS film decayed exponentially. The experimentally obtained corrected decay profile could thus be expressed in the following functional form[26,27]

$$I(t) = Ae^{-t/\tau}\int_{-\infty}^{t} S(t')e^{t'/\tau}\,dt' \qquad (3)$$

in which $I(t)$ is the fluorescence intensity as a function of time, and A and τ, the fluorescence lifetime, are parameters. $S(t)$ is the intensity of a scattered laser pulse as a function of time and was obtained experimentally by scattering the exciting pulse off a dilute solution of nondairy coffee creamer in water. $S(t)$ was obtained by using the same optical configuration as used to obtain $I(t)$ so that the position of $t = 0$ in $I(t)$ (the time position corresponding to the peak of the excitation pulse) could be determined precisely. This was accomplished by aligning the marker pulse of the $S(t)$ file with the marker pulse of the $I(t)$ file. A linear least-squares fit of the Taylor series expansion to first order in the two parameters[28] of the above function, which is a convolution

(24) Bevington, P. R. *Data Reduction and Error Analysis for the Physical Sciences*; McGraw-Hill: New York, 1969.

(25) Phillips, L. A. Picosecond studies of structure and dynamics of electronically excited molecules in solution. Ph.D. Thesis, Lawrence Berkeley Laboratory, University of California, Berkeley, 1985, p 104.

(26) Haug, A.; Kohler, B. E.; Priestley, E. B.; Robinson, G. W. Measurement of rapid processes using a modulated cw laser. *Rev. Sci. Instrum.* **1969**, *40*, 1439–1444.

(27) Huston, A. L.; Scott, G. W.; Gupta, A. Mechanism and kinetics of excited-state relaxation in internally hydrogen-bonded molecules: 2-(2'-hydroxy-5'-methylphenyl)-benzotriazole in solution. *J. Chem. Phys.* **1982**, *76*, 4978–85.

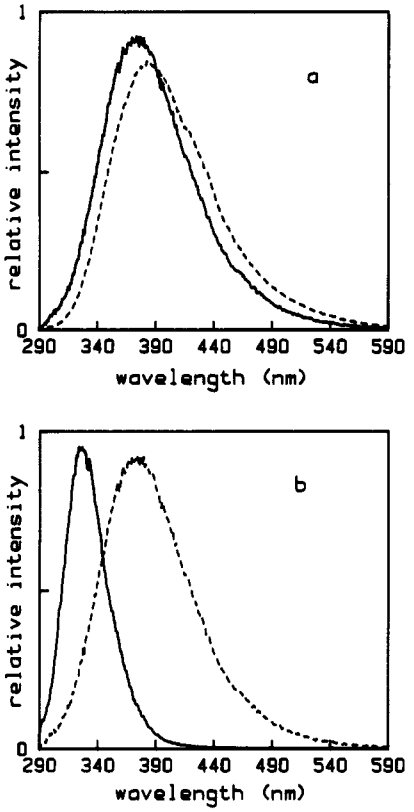

Figure 3. (a) Steady-state room temperature emission spectra of dilute pentafluorotoluene (---) and PPFS film (—) (λ_{ex} = 270 nm). (b) Room temperature emission spectra of PS film (—) and PPFS film (---) (λ_{ex} = 266 nm).

of the detector response to the scattered laser pulse and the fluorescence of the sample, to a corrected decay profile was then done iteratively until the minimum in the root-mean-square value was obtained.

3. Results and Discussion

3.1. Absorption Spectra. The UV absorption spectra of a PPFS film and a dilute solution of PPFS in ethyl acetate are shown in Figure 2a. These spectra both show a weak band with a maximum at 259 nm (ϵ = 325 cm^{-1} M^{-1} in ethyl acetate). The absorption spectrum of 10^{-5} M PFT in pentane (Figure 2b) has a similar weak band (ϵ = 456 cm^{-1} M^{-1} at 260 nm). The location of this band is similar to phenyl π–π^* absorptions such as are seen in spectra of benzene and polystyrene (see Figure 2b). However, the lack of vibronic structure in the absorption spectra of PPFS and PFT is unlike benzene and polystyrene, but very similar to the absorption spectra of pentafluorobenzene and hexafluorobenzene.[15]

3.2. Steady-State Emission Spectra and Fluorescence Excitation Spectra. The room temperature steady-state emission spectra of PPFS film and PFT in pentane (10^{-5} M) are shown in Figure 3a. A neat solution of PFT exhibits a nearly identical emission spectrum as the dilute solution. The room temperature steady-state emission spectra of PPFS film and PS film are shown in Figure 3b. The room temperature emission spectra of PFT and PPFS are independent of excitation wavelength for energies above their respective 0–0 absorption bands. The structureless, highly Stokes shifted band (λ_{max} = 375 nm) seen in both the spectra of PPFS film and PFT is very similar to the emission spectrum observed for pentafluorobenzene.[15] The fact that the features of the PFT emission spectra do not show a concentration dependence suggests this emission is not due to excimers. Furthermore, the Stokes shift between the Franck–Condon maximum of the emission and the 0–0 absorption band for both PFT and PPFS is approximately 10 000 cm^{-1}. However, it is known that the

(28) See ref 24, Chapter 11, pp 232–239.

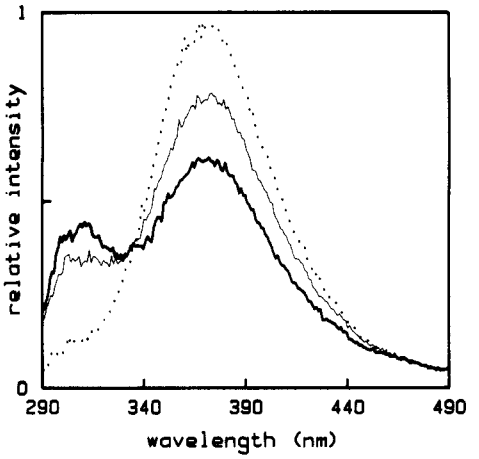

Figure 4. Steady-state emission spectra of PPFS film at 11 K resulting from excitation at 272 nm (bold —), 271 nm (light —), and 268 nm (···). Note the isoemissive point at 334 nm.

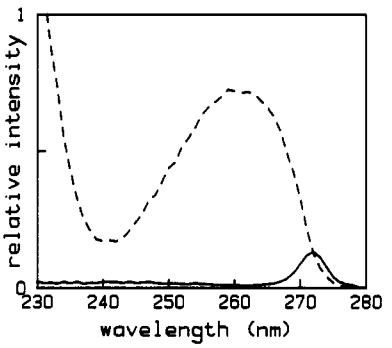

Figure 5. Fluorescence excitation spectra of PPFS thin film at 11 K monitoring the 310-nm emission band (—) and the 375-nm emission band (---).

Stokes shift of excimers formed from aromatic compounds[29] is more typically ~6000 cm^{-1}. For example, the excimer emission band of polystyrene is centered near 325 nm (see Figure 3b) while its 0–0 absorption is at 271 nm (Stokes shift $\simeq$ 6100 cm^{-1}). The normal, Stokes-shifted monomer emission band of PS film is centered near 290 nm and is weak at room temperature (see Figure 3b). There is no detectable emission from PPFS film or PFT below 290 nm. We therefore conclude that the broad, structureless emission band (λ_{El} = 375 nm) of PFT and of PPFS film at room temperature is not due to an excimer but rather is due to an excited-state conformation which is significantly distorted from the initially excited ground-state conformation. This conclusion is consistent with the interpretation of the emission of pentafluorobenzene[15,23] and hexafluorobenzene.[16,17,23]

The emission spectra of PPFS film held at 11 K resulting from excitation at three different wavelengths (268, 271, and 272 nm) are shown in Figure 4. In this case, *two* overlapping emission bands are observed at 11 K. One of them, the lower energy, structureless, more highly Stokes-shifted band (λ_{max} = 375 nm) was also observed at room temperature. The higher energy band (λ_{max} = 310 nm) was not evident at room temperature. A most interesting feature of these spectra is the presence of the isoemissive point at 334 nm with the concomitant increase of intensity of the higher energy band and decrease of intensity of the lower energy band as the excitation energy is decreased.

The fluorescence excitation spectra monitored at two emission wavelengths of a very thin PPFS film at 11 K are shown in Figure 5. The spectrum obtained by monitoring the lower energy emission (λ = 375 nm) resembles the absorption spectrum of the PPFS film absorption (see Figure 2). However, the spectrum monitoring the higher energy emission (λ = 310 nm) shows sig-

(29) Birks, J. B. *Photophysics of Aromatic Molecules*; Wiley-Interscience: London, 1970; p 354.

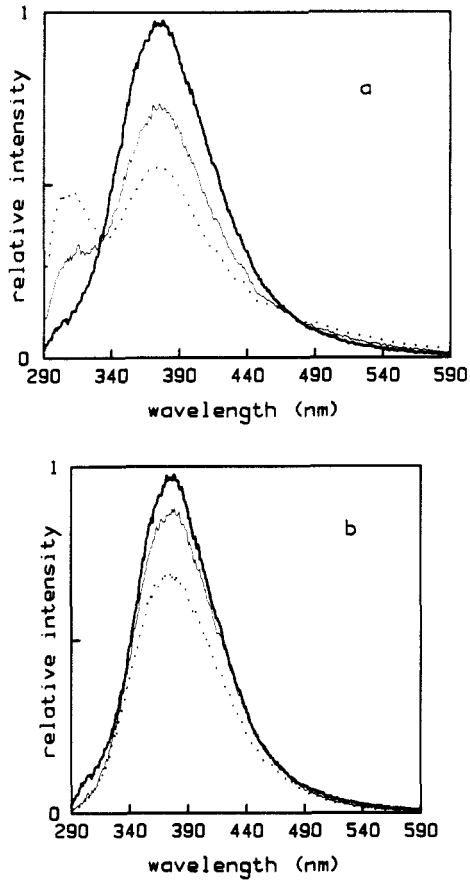

Figure 6. Steady-state emission spectra of PPFS film excited with 273-nm photons as a function of temperature: (a) 15 K (···), 99 K (light —), 188 K (bold —); (b) 188 K (bold —), 255 K (light —), 296 K (···).

nificant intensity only near the red edge of the PPFS film absorption. Clearly, emission in both energy regions can be seen simultaneously only with excitation near the red edge of the absorption band.

The two bands in the 11 K emission spectrum of PPFS film, as well as the fluorescence excitation spectra of these bands at 11 K, indicate the presence of two different emitting electronic states or conformations. (From now on we will simply refer to these as two fluorescing states, bearing in mind that two distinct species or conformations may be responsible for dual emission.) The isoemissive point at 334 nm resulting from the variation in excitation energy indicates that these two entities are interconverting. If we assume that the total number of excited molecules does not vary with excitation wavelength over the range 268–273 nm, (this assumption is based on the fact that the optical density of these films is greater than two throughout this wavelength range) then we can conclude that the quantum yield of emission of the two states is equal at 334 nm.[30]

The temperature dependence of the emission spectrum of PPFS film excited at 273 nm is shown in Figure 6. At this excitation wavelength and below 188 K, the intensity of the higher energy emission band, λ_{E2} = 310 nm, increases with decreasing temperature while the intensity of the lower energy band, λ_{E1} = 375 nm, decreases with decreasing temperature. This also results, in the temperature-dependent spectra over the range of 4–188 K, in an isoemissive point at 334 nm, the same wavelength as the isoemissive point in the excitation wavelength dependent spectra at 11 K (see Figure 4). In addition, the emission intensity in the spectral region of $\lambda > 472$ nm increases with decreasing temperature over the range of 4–188 K, similarly to the behavior of the higher energy band. This results in a second isoemissive point at 472 nm. At temperatures greater than 188 K, the emission intensity of the spectrum decreases monotonically with increasing

(30) Cohen, M. D.; Fischer, E. Isobestic Points. *J. Chem. Soc.* **1962**, 3044.

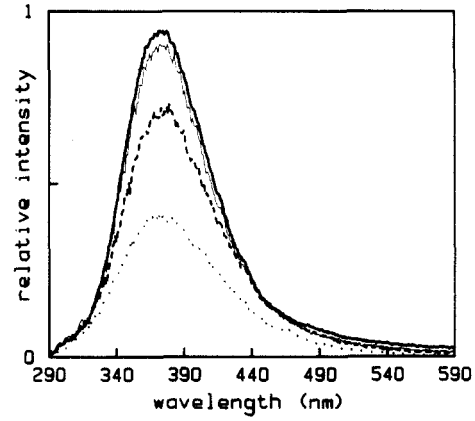

Figure 7. Steady-state emission spectra of PPFS film excited with 250-nm photons as a function of temperature: 15 K (bold —), 29 K (light —), 148 K (---), 296 K (···).

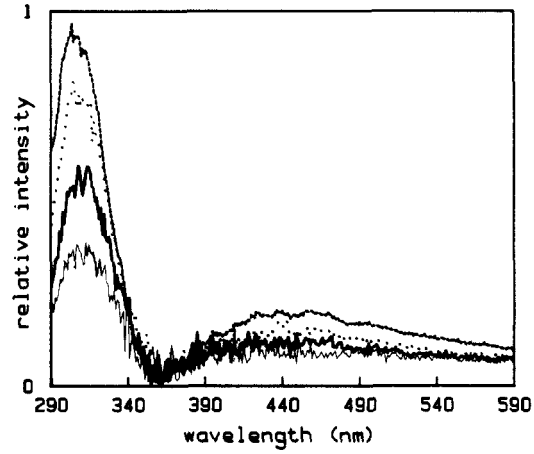

Figure 8. PPFS emission spectra resulting from only the higher energy state, λ_{max} = 310 nm, as a function of temperature: 4 K (---), 29 K (···), 82 K (bold —), 116 K (light —). See text for explanation of derivation of these spectra.

temperature throughout the entire spectral range as seen in Figure 6b.

The isoemissive point at 334 nm observed in these spectra of PPFS film excited at 273 nm over the temperature range 2–188 K is a further indication of two interconverting excited electronic states or species. The presence of this isoemissive point over this large temperature range indicates that not only are the quantum yields of emission of the two states equal at 334 nm, but also the quantum yields of both states are essentially temperature independent over this range. This conclusion is based on the fact that the isoemissive point indicates a constant steady-state total population of fluorescing states.[30]

The temperature dependence of the PPFS film emission excited at 250 nm is shown in Figure 7. There is no indication of the higher energy emission band, λ_{E2} = 310 nm, at any temperature when exciting at this wavelength. The features of these spectra at all temperatures are essentially the same as those of the room temperature spectrum with a single structureless, highly Stokes-shifted band centered near 375 nm. The emission intensity increases monotonically with decreasing temperature. We therefore conclude that the emission spectra shown in Figure 7 are due to the lower energy state only.

While the emission spectra of the lower energy state of PPFS film as a function of temperature are shown in Figure 7, the emission spectra of *both* the lower energy and the higher energy state are shown in Figure 6. In order to obtain the emission spectrum of only the higher energy state, the following procedure was used. It was assumed that the emission intensity at 378 nm resulting from 273-nm excitation (Figure 6) was due solely to the lower energy emissive state. Since the spectra of Figure 7 are due solely to this lower energy state, the spectrum at a given

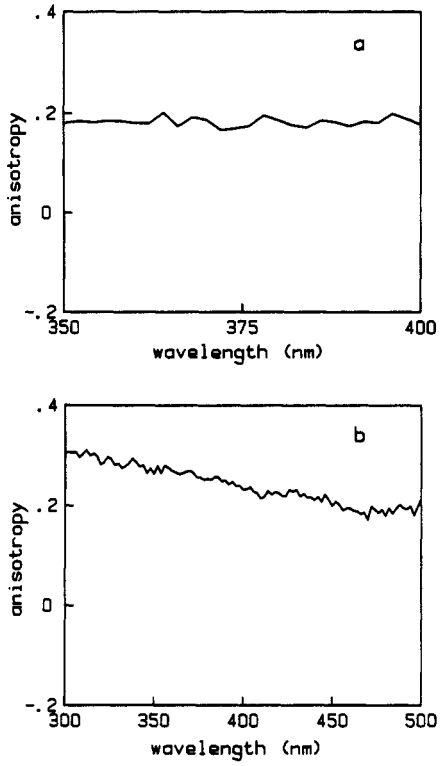

Figure 9. Steady-state fluorescence anisotropy of PPFS film at (a) room temperature and (b) 14 K, λ_{ex} = 273 nm. The room temperature anisotropy is independent of excitation wavelength.

temperature in Figure 7 was subtracted from the spectrum of the corresponding temperature in Figure 6 after normalizing the intensity values at 378 nm. The resulting difference spectra are shown in Figure 8. Two emission bands are seen and both decrease monotonically with increasing temperature. The emission lifetime of the band centered near 500 nm was found to be ~4 s at 14 K. We therefore conclude that this emission is the phosphorescence from a triplet state associated with the state which gives rise to the higher energy fluorescence. It is the overlap of this phosphorescence with the fluorescence of the lower energy state that results in a second isoemissive point at 472 nm in Figure 6. The fluorescence band of this higher energy state is significantly red-shifted from the absorption spectrum of PPFS; i.e., its maximum is near 310 nm. This is unlike the emission of benzene, whose fluorescence maximum is near 290 nm, and again indicates that this excited state is also distorted significantly relative to the ground state, albeit not as much as the lower energy state.

3.3. Emission Polarization Anisotropy Spectra. The emission polarization anisotropy spectrum of PPFS film at room temperature is shown in Figure 9a. The room temperature anisotropy value of $r = 0.18 \pm 0.02$ is independent of excitation wavelength from the red edge of the absorption band to at least 260 nm. The emission polarization anisotropy is also constant, within experimental uncertainty, throughout the entire room temperature spectrum. This is the expected result of a single emissive excited state.[31] The emission anisotropy spectrum of PPFS film excited at 273 nm at 14 K is shown in Figure 9b. This emission polarization anisotropy decreases significantly in going from 300 to 400 nm. This wavelength dependence of the emission anisotropy offers further evidence of the existence of the two emissive states[31] as proposed above.

The emission polarization anisotropy of PS film was recorded at room temperature and 14 K as well. The polarization anisotropy of PS emission was constant within experimental error throughout the emission spectrum at both 296 and 14 K in spite of the fact that two species are responsible for the emission, namely the excimer and monomer. Efficient electronic energy transfer in

(31) Lakowicz, J. R. *Principles of Fluorescence Spectroscopy*; Plenum Press: New York, 1983; Chapter 5.

TABLE I: Emission Anisotropy of Polymer Films

	poly(2,3,4,5,6-pentafluorostyrene)		polystyrene	
	310 nm	380 nm	monomer	excimer
14 K	0.30 ± 0.02	0.23 ± 0.02	0.02 ± 0.02	0.02 ± 0.02
296 K		0.18 ± 0.02		0.02 ± 0.02

TABLE II: Poly(2,3,4,5,6-pentafluorostyrene) Film Fluorescence Lifetimes as a Function of Temperature Excited at 266 nm

T, K	τ, ns	T, K	τ, ns
296	1.78 ± 0.1	99	2.65 ± 0.1
229	2.20 ± 0.1	60	2.75 ± 0.1
181	2.55 ± 0.1	29	2.74 ± 0.1
147	2.60 ± 0.1	14	2.77 ± 0.1

polystyrene film results in depolarization of the emission for both the monomer and excimer.[32,33] (Natural light has an anisotropy value of $r = 0$.)

A summary of the emission polarization anisotropy results is shown in Table I. The uncertainties of these values (0.02) was estimated from the observed variation in polarization anisotropy values of portions of the same polymer film recorded at different times. This variation is also consistent with previously reported results on polymer films.[32,33]

3.4. Fluorescence Lifetimes. The temperature dependence of the fluorescence lifetimes of PPFS film is summarized in Table II. Within experimental error, the fluorescence lifetime of the lower energy state (λ_{E1} = 375 nm) remains essentially constant with decreasing temperature below 181 K. This suggests that the quantum yield of emission should remain constant over this range as well since $\Phi = k_r\tau$, where Φ is the quantum yield, k_r the pure radiative rate constant, and τ the fluorescence lifetime. The constancy of the quantum yield over this temperature range was proposed in section 3.2 based on the presence of the isoemissive point in the temperature-dependent spectra of PPFS film excited at 273 nm.

Analysis of fluorescence decay profiles obtained by collecting the emission through a higher energy wavelength cutoff filter (Schott WG305) yielded fluorescence lifetimes that were the same as those reported within experimental error. This result is to be expected since, even at low temperatures, the amount of emission from the higher energy state, λ_{E2} = 310 nm, is relatively small when excited at 266 nm (see Figure 5).

4. Analysis

4.1. Higher Energy State. The temperature dependence and excitation energy dependence of the relative emission intensity from the two fluorescing states is indicative of an energy barrier between the two. We can obtain an estimate of the energy barrier height from our data by assuming the following photophysical model for the lower energy state. We assume that

$$\Phi(T) = k_r/(k_r + k_{nr} + k(T)) \tag{4a}$$

in which $\Phi(T)$ is the fluorescence quantum yield, k_r and k_{nr} are the temperature-independent pure radiative rate constant and nonradiative rate constant, and $k(T)$ is a temperature-dependent rate of deactivation of the excited state. It follows that

$$k(T) - k(4\text{ K}) = k_r\{1/\Phi_{rel} - 1\}/\Phi(4\text{ K}) \tag{4b}$$

in which $\Phi_{rel} = \Phi(T)/\Phi(4)$. Thus,

$$\Phi_{rel} = \{1 + [\Phi(4)/k_r](k(T) - k(4))\}^{-1} \tag{5}$$

If we now assume that there are two temperature-dependent nonradiative decay pathways available to the higher energy state, namely to the lower energy fluorescing state, $k_{h\to l}(T)$, and to the

(32) Gupta, M. C.; Gupta, A.; Horowitz, J.; Kliger, D. Time-resolved fluorescence and emission depolarization studies of polystyrene: photochemical processes in polymeric systems. 9. *Macromolecules* **1982**, *15*, 1372–76.

(33) Putnam-deLavareille, N.; Geuskens, G. Luminescence studies of polymers-IX: polarization of the fluorescence of copolymer films. *Eur. Polym. J.* **1977**, *13*, 15–16.

TABLE III: Temperature-Dependent Relative Emission Intensities of the Higher Energy State of Poly(2,3,4,5,6-pentafluorostyrene) Film

T, K	Φ_{rel}	T, K	Φ_{rel}	T, K	Φ_{rel}
4	1.0	44	0.78	116	0.36
11	0.98	60	0.72	148	0.19
15	0.93	82	0.59	188	0.06
29	0.85	99	0.50		

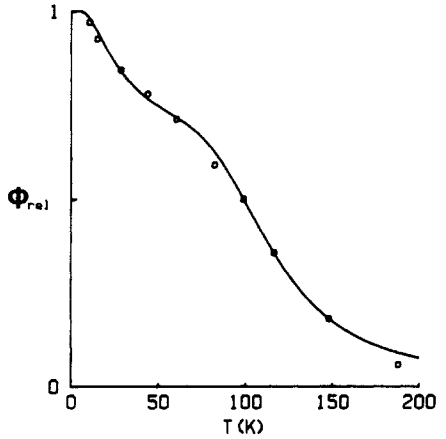

Figure 10. Plot of relative fluorescence quantum yield Φ_{rel} of the higher energy state of PPFS film as a function of temperature and the best fit (—) of eq 7 to the data (O).

ground state, $k_{nr}(T)$, and we further assume that both of these rate constants follow an Arrhenius rate law, then we can write

$$k(T) = k_{nr}(T) + k_{h\to l}(T) = Ae^{-E_l/RT} + Be^{-E_{h\to l}/RT} \quad (6)$$

In this expression, E_l is the activation energy for nonradiative decay to the ground state and $E_{h\to l}$ is the activation energy or barrier height for conversion from the higher energy fluorescing state to the lower energy fluorescing state. Substituting this expression into eq 5 yields the following expression relating the relative quantum yield Φ_{rel} to the temperature:

$$\Phi_{rel} = \{1 + [\Phi(4)/k_r] \times (Ae^{-E_l/RT} - Ae^{-E_l/R\cdot4} + Be^{-E_{h\to l}/RT} - Be^{-E_{h\to l}/R\cdot4})\}^{-1} \quad (7)$$

Since the quantum yield is directly proportional to the integrated intensity of the emission spectrum, $\Phi_{rel} = I(T)/I(4\text{ K})$, where $I(T)$ is the integrated intensity (290–350 nm) of the higher energy emission band at temperature T obtained from the spectra of Figure 8. Table III summarizes Φ_{rel} for all temperatures investigated. A four-parameter fit[34-36] of eq 7 to this data resulted in a barrier height of $E_{h\to l}/hc = 27 \pm 7$ cm^{-1} and an activation energy for nonradiative internal conversion of $E_l/hc = 425 \pm 40$ cm^{-1}. A plot of the best fit of eq 7 to the data is shown in Figure 10.

4.2. Lower Energy State. The temperature dependence of the fluorescence lifetime of the lower energy state (see Table II) can be used to obtain an estimate of the activation energy for nonradiative decay from this state to the ground state. We begin with an expression of the fluorescence lifetime

$$1/\tau(T) = k_r + k_{nr} + k_{nr}(T) \quad (8)$$

in which k_r and k_{nr} are the temperature-independent pure radiative rate constant and temperature-independent nonradiative decay rate constant, respectively. $\tau(T)$ is the fluorescence lifetime at temperature T, and $k_{nr}(T)$ is the temperature-dependent rate

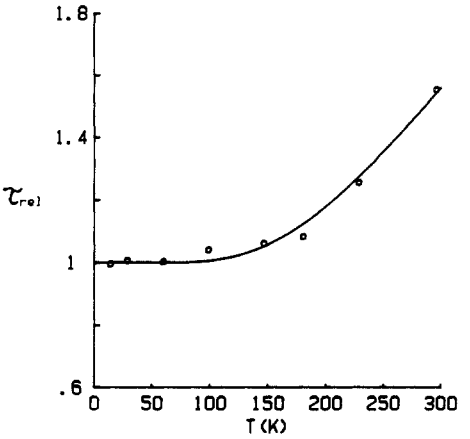

Figure 11. Plot of relative fluorescence lifetime τ_{rel} of the lower energy state of PPFS film as a function of temperature and the best fit (—) of eq 10 to the data (O).

constant of internal conversion from this excited state. If we assume again that $k_{nr}(T)$ is given by the Arrhenius expression

$$k_{nr}(T) = Ae^{-E/RT} \quad (9)$$

in which E is the activation energy and A is the frequency factor, then we can write

$$\tau_{rel} = 1 + \tau(14)A(e^{-E/RT} - e^{-E/R\cdot14}) \quad (10)$$

in which $\tau_{rel} = \tau(14)/\tau(\text{K})$. Implicit in our expression (9) for the nonradiative decay rate is the assumption that the rate of conversion of the lower energy state to the higher energy state is not significant. This is supported by the fact that the steady-state emission spectrum of PPFS film excited at 266 nm does not exhibit the band near 310 nm associated with the higher energy state. A two-parameter (E and $\tau(14)A$) nonlinear least-squares fit[34-36] of eq 10 to the fluorescence lifetime data of Table II yielded an activation energy given by $E/hc = 477 \pm 30$ cm^{-1} and a value of $\tau(14)A = 5.6 \pm 0.7$. Substituting our value of $\tau(14) = 2.77 \pm 0.1$ ns from Table II, we calculate a preexponential frequency factor of $A = (2.0 \pm 0.3) \times 10^9$ s^{-1}. The plot of the best fit of eq 10 to the data is shown in Figure 11. This rather large activation energy is consistent with the proposition made earlier that the quantum yield and hence the fluorescence lifetime for the lower energy state of PPFS film would be essentially temperature independent over the range of 4–180 K. That is, eq 9 predicts that $k_{nr}(4) = 0$ and, thus, $k_r + k_{nr} = 1/\tau(4) = 3.6 \times 10^8$ s^{-1} and $\Phi(188)/\Phi(4) = 0.9$. It should also be noted that the activation energies for nonradiative decay from the higher energy state and the lower energy state are the same within experimental error.

4.3. Angle between Absorption and Emission Transition Dipoles. The fluorescence anisotropy of randomly oriented chromophores which have both single axis absorption and emission dipoles has a maximum value[31] of $r = 0.4$. A value less than this can be the result of, for example, (1) rotational motion of the chromophores during the excited-state lifetime, (2) electronic energy transfer between chromophores with nonparallel transition dipoles, or (3) an angular difference between the absorption and emission transition dipoles. The anisotropy value of essentially zero for PS film (see Table I) is believed to be largely the result of process 2, i.e., several electronic energy transfer steps among phenyl chromophores prior to emission.[9,32] One essential requirement of energy transfer is the overlap of the emission spectrum of the donor with the absorption spectrum of the acceptor[1] as is the case for the polystyrene monomer with itself.[37] Since the emission spectrum of the lower energy state in PPFS is highly red-shifted from the absorption spectrum, electronic energy transfer from this state is not possible. We see in Figure

(34) Caceci, M. S.; Cacheris, W. P. Fitting curves to data: the Simplex algorithm is the answer. *BYTE*, **1984**, 340–363.

(35) Noggle, J. H. *Physical Chemistry on a Microcomputer*; Little, Brown & Co: New York, 1985; pp 148–165.

(36) The Simplex nonlinear least-squares fitting algorithm used to fit eqs 7 and 10 to the data finds the minimum standard deviation in parameter space. The reported uncertainties in each parameter were obtained by fixing all parameters at their optimum values except the one of interest and determining the variation in that parameter which resulted in a 2-fold increase in the minimum standard deviation.[35]

(37) Polacki, Z. Some remarks on donor properties of polystyrene. *J. Photochem.* **1985**, *28*, 135.

8 that the emission spectrum of even the higher energy fluorescing state in PPFS film is significantly red-shifted from the absorption spectrum and, therefore, electronic energy transfer is not likely from this state either. Therefore, we would not expect electronic energy migration to occur in this PPFS polymer film and the much larger anisotropy value of PPFS film compared to PS film provides significant support for this viewpoint. Furthermore, the fact that the anisotropy of PPFS film is less than 0.4 cannot be the result of process 1, rotational motion. From Table I it is seen that the anisotropy of the lower energy emissive state of PPFS changes by only 0.05 in going from room temperature to 14 K. This indicates that rotational motion of the chromophores is not a significant factor in depolarizing of the emission, especially at 14 K. We therefore assert that the anisotropy value of less than 0.4 of PPFS film is due to the angular difference between the absorption and emission dipoles of the chromophores. The angular dependence of anisotropy is given by the following expression

$$r = 0.2(3\cos^2\alpha - 1) \quad (11)$$

in which α is the angle between the absorption and emission dipoles of the chromophore. Solving this expression for α using the anisotropy values of the PPFS film at 14 K of Table I yields angles of 24 ± 2° and 32 ± 2° between the absorption and emission dipoles of the higher energy state and lower energy state, respectively. These results support the notion that the higher and lower energy fluorescing states represent progressive chromophore geometry distortions from the ground-state geometry which is reflected by the absorption transition dipole. Apparently these distortions result in rotation of the transition dipoles as well lowering of the excited-state energy.

5. Conclusions

The results of the temperature-dependent steady-state fluorescence, fluorescence polarization anisotropy, and fluorescence lifetime of PPFS film have led to the following conclusions:

(1) Electronic energy migration does not occur in this polymer.

(2) At room temperature, the highly Stokes-shifted fluorescence is associated with an excited-state conformation which is greatly distorted from the ground-state geometry.

(3) Two interconverting excited-state conformers contribute to the emission spectra at temperatures below 180 K with excitation energies near the 0–0 absorption band of the polymer. The lower energy conformer is the same as attributed to the room temperature fluorescence. The higher energy conformer is also distorted significantly from the ground-state geometry. The internal conversion of either of these conformers to the ground state is essentially a temperature-independent process below 180 K.

Acknowledgment. This research was supported, in part, by the Committee on Research, University of California, Riverside. Work at the Jet Propulsion Laboratory, California Institute of Technology, was performed under contract with the National Aeronautics and Space Administration.

Registry No. PPFS, 26838-55-1; PFT, 771-56-2; PS, 9003-53-6.

Preparation of a High-Quality Source and Reference Standard for ^{129}Xe Mössbauer Spectroscopy

Thomas Birchall,† Christopher S. Frampton, Gary J. Schrobilgen,* and Jónína Valsdóttir

Department of Chemistry, McMaster University, Hamilton, Ontario, L8S 4M1 Canada
(Received: February 5, 1990)

Pentasodium orthoperiodate, $Na_5{}^{129}IO_6$, has been prepared for use as a source in ^{129}Xe Mössbauer spectroscopy. Raman and ^{127}I Mössbauer spectroscopy, along with chemical analysis, were used to characterize the compound. The high recoil-free fraction and narrow line width, 7.2–7.3 mm/s, demonstrate the merits of $Na_5{}^{129}IO_6$ compared to previously used sources. A high-yield preparation of the ^{129}Xe reference standard, β-hydroquinone xenon clathrate, $3C_6H_4(OH)_2{\cdot}0.92Xe$, is also described.

Introduction

The precursor for the Mössbauer effect in ^{129}Xe is the artificial radioactive isotope ^{129}I, $t_{1/2} = 1.57 \times 10^7$ yr, which populates the 39.6-keV level of the first excited state of xenon through β-decay.[1] Xenon-129 Mössbauer spectroscopy has been used as a probe to examine the bonding properties of xenon compounds since the inception of noble-gas chemistry in 1962.[2] The main emphasis has been on using the compounds of interest as absorbers, but several experiments have been carried out using the emission technique where the xenon compound is formed by the β-decay of an isoelectronic ^{129}I analogue. This is, to date, the only known method to synthesize and characterize the highly unstable xenon halides, $XeCl_2$, $XeCl_4$, and $XeBr_2$.[3,4]

The accuracy of the information obtained from a Mössbauer spectrum depends heavily upon the quality of the source. A number of ^{129}I compounds have served as single-line sources for ^{129}Xe Mössbauer spectroscopy, i.e., $Na^{129}I$, $K^{129}IO_4$, and $Na_2H_3{}^{129}IO_6$.[3] Sodium trihydrogen orthoperiodate is the most recently used source,[5] as it exhibits the largest absorbance and thereby partially compensates for the low count rate inherent in ^{129}Xe Mössbauer spectroscopy.[6,7] It has the disadvantage of broad lines; the width of the narrowest line observed was 8.8 mm/s, while the natural line width is 6.8 mm/s (determined from the half-life of the excited state). The multiline pattern in the ^{129}I Mössbauer spectrum of this compound showed that line broadening was caused by a quadrupole interaction at the iodine nucleus.[8] In

* To whom correspondence should be addressed.
† Deceased April 29, 1990.

(1) Stevens, J. G.; Stevens, V. E., Eds.; *Mössbauer Effect Data Index, For 1976 Literature*; IFI/Plenum: New York, 1978; p 164.
(2) (a) Perlow, G. J. *Chemical Applications of Mössbauer Spectroscopy*; Goldanskii, V. I., Herber, R. H., Eds.; Academic Press: New York, 1968; p 377. (b) Greenwood, N. N.; Gibb, T. C. *Mössbauer Spectroscopy*; Chapman and Hall: London, 1971; p 482.
(3) Perlow, G. J.; Perlow, M. R. *J. Chem. Phys.* **1968**, *48*, 955.
(4) Perlow, G. J.; Yoshida, H. *J. Chem. Phys.* **1968**, *49*, 1474.
(5) de Waard, H.; Bukshpan, S.; Schrobilgen, G. J.; Holloway, J. H.; Martin, D. *J. Chem. Phys.* **1979**, *70*, 3247.
(6) For the sake of consistency the formulation $Na_2H_3IO_6$ is used throughout, but the controversy regarding $Na_2H_3IO_6$ versus $Na_3H_2IO_6$ is discussed in ref 7.
(7) Batchelor, R. J.; Birchall, T.; Myers, R. D. *J. Chem. Phys.* **1982**, *77*, 3383, and references therein.

0022-3654/90/2094-6503$02.50/0